VALIDATION BY EXPERIMENTS FOR GAS ENTRAINMENT STUDIES IN 5/8 SURGE TANK MODEL OF PFBR

D.Ramdasu, N.S.Shivakumar, G.Padmakumar, C.AnandBabu, G.Vaidyanathan

Fast Reactor Technology Group, Indira Gandhi Centre for Atomic Research
Kalpakkam, India -603102, Phone No & Fax: 044 -27480086

S.Rammohan, S.K Sreekala, S.Manikandan, S.Saseendran

Fluid Control Research Institute, Palghat, India-678623,
Phone No: 0491-256120, Fax: 0491-2566326

Abstract

A Surge tank is provided in the secondary circuit of typical sodium cooled fast breeder reactor, to take care of pressure surges in case of a sodium water reaction in Steam Generators (SG). The blanket of argon cover gas at the top of the tank acts as a cushion for the surges. The argon gas above the free surface of sodium in the tank is a source of entrainment into the sodium which is undesirable from the consideration of effective heat transfer in Intermediate Heat Exchanger (IHX), SG, and cavitation in pumps. To investigate the phenomenon of gas entrainment in surge tank, Computational Fluid Dynamics (CFD) analysis was carried out simulating the model geometry for single phase and two-phase flows. Initially velocity mapping in surge tank was carried out without any devices and later with internal devices of different geometries. Based on these, the cases where the free surface velocities were minimal was investigated experimentally. The experiments were conducted in a 5/8 scale model surge tank simulating Weber and Froude numbers. This paper discusses the computational model, experimental methodology, results & the discussion on the result.

1.0 INTRODUCTION

A 500 MWe capacity sodium cooled fast breeder reactor (PFBR) is currently under construction at Kalpakkam, India. The heart of the reactor is the core where heat is generated from nuclear fission. This heat is transported by primary sodium and transfers the heat to the secondary sodium in the Intermediate Heat Exchanger (IHX). From IHX, secondary sodium travels through surge tank and exchanges heat to the water in the tubes of the steam generator as shown in Fig.1.

In case of leak in the Steam Generator tubes, high pressure water would leak into the sodium causing a sodium water reaction which results in high pressure surges due to generation of hydrogen. Pressure surges are also possible due to inadvertent closure of isolation valves. In order to protect IHX from the effect of these pressure surges a surge tank is provided in the hot leg. The pump tank (SSP in Fig.1) serves as the surge absorber in the cold leg of the secondary sodium circuit. Surge tank is a cylindrical vessel with torispherical dished closures at both ends.

The secondary sodium from the IHX outlet enters into the surge tank through two inlet nozzles Argon fills the space above free surface of sodium and provides cushion in case of pressure surges. The pressure of argon gas in surge tank is maintained at 0.4 MPa. Sodium exits from the surge tank through the four outlet nozzles to four steam generator modules and returns to IHX through the secondary sodium pump. The entrainment of argon gas from the surge tank in to the secondary sodium system is an undesirable phenomenon from the consideration of effective heat transfer in Intermediate Heat Exchanger (IHX) and SG, cavitation in pumps and operational

problems of continuous feed and bleed of cover gas, thus leading to unfavourable reactor operating conditions.

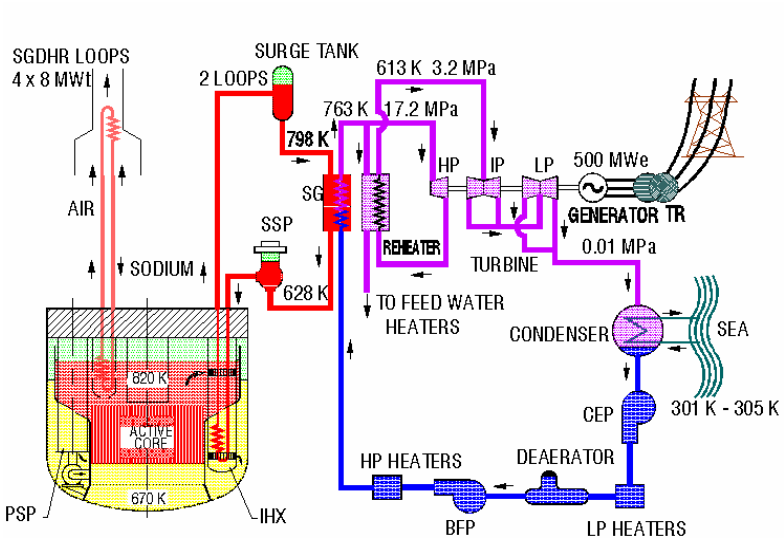

Fig.1 Schematic of PFBR Heat transport circuit

The understanding and prediction of gas entrainment phenomenon computationally and experimentally will aid in the design of the surge tank. The objective of the present investigation is to computationally determine the condition for onset of gas entrainment from the free surface into the pool of liquid sodium in the surge tank. The flow profile in the surge tank influences the gas entrainment mechanisms. The velocity profile pattern in the surge tank is modeled using CFD. The CFD analysis also was beneficial in reducing the experimental trials for testing various device configurations.

The scope of the experiments mainly focuses on establishing the minimum height required to avoid gas entrainment by means of internal devices that could be deployed in the surge tank and thereby reduce the liquid sodium inventory and tank height. The results from these experiments will help in optimizing the design of devices that could be used to mitigate gas entrainment for PFBR.

This paper presents the, similitude criteria, scale model chosen and results of the experiments and different devices to mitigate gas entrainment in the models and compared with CFD results.

2.0 SIMILARITY CRITERIA

Gas entrainment phenomenon depends upon viscous forces, gravity forces and surface tension forces. Surface tension and gravity forces are characterized by Weber Number and Froude Number respectively. These are the two predominant non dimensional numbers that has to be maintained equal to the prototype while maintaining the flow in the turbulent regime for determining the onset of entrainment. The definition of Froude number and Weber number are as follows.

Froude number = Inertia force/Gravity force, $$\left(\frac{V^2}{Lg}\right)_m = \left(\frac{V^2}{Lg}\right)_p \quad (1)$$

Weber Number = Inertial force /Surface tension force, $$\left(\frac{\rho L V^2}{\sigma}\right)_m = \left(\frac{\rho L V^2}{\sigma}\right)_p \quad (2)$$

Where
V = Velocity (m/s)
L = Characteristic length (m)
s = Surface tension (N/m)
ρ = Density (kg / m^3)

and subscript 'm' and 'p' denotes model and prototype respectively.

In the model experiment both the above numbers were simulated and the scale size was found to be 5/8.

3.0 NUMERICAL STUDIES ON GAS ENTRAINMENT

Numerical simulations analyzing the phenomenon of gas entrainment in the LMFBR pool have been reported. The free surface of a top entry loop type LMFBR in Japan has been numerically simulated (Gao Ming Qing, 1997). The analyses carried out with the AQUA-VOF code investigated the efficiency of the ring plate's placed, 1m below the free surface. The results show that the ring plates have sufficiently high potential to eliminate the free surface gradients. The maximum free surface height difference and the maximum gradient free surface were decreased to less than15%, and 64% compared with the case with out ring plates respectively.

Two dimensional waterfall numerical simulations and a three- dimensional dimple simulation for the gas entrainment and bubble transport from free to the hot leg of a fast breeder nuclear reactor have been reported(Tomoaki Kunugi, 2005). The analysis carried out using the MARS (Multi-Interface and Advection and Reconstruction Solver) method was found to be useful in capturing flow modes in the vortex – dimple evolution. These numerical results were compared to the experimental results and found that surface velocity and the time averaged wave shape were found to be very similar to the experimental findings. The phenomenon of gas entrainment in the PFBR surge tank has been analyzed numerically. The CFD analysis was used to determine free surface velocity distribution in surge tank. The analysis also was helpful in finalizing the devices to be used in experimental model thereby minimizing experimental trials.

4.0 MODELING DETAILS

Fig. 2 shows the geometry of the surge tank considered for the modeling. It is a 5/8 scale model of the surge tank with two inlets with diameter of ϕ333mm (D_{in}), four equispaced outlets with diameter of ϕ253mm (D_{out}) and tank diameter of ϕ1414.6mm. For computational purpose upstream pipe of $10D_{in}$ long and down stream pipes of $10D_{out}$ long is considered.

Tetrahedral meshing is done inside the tank and hexahedral meshing is done for the outlets. Total of 1,814,143 cells are used for meshing the whole computational domain. Aspect ratio ranges from 1 to 5 and skewness is less than 0.3. Fine meshing is done at bottom of the dish, near the inlet, pepper pot and at the entrance to the outlet

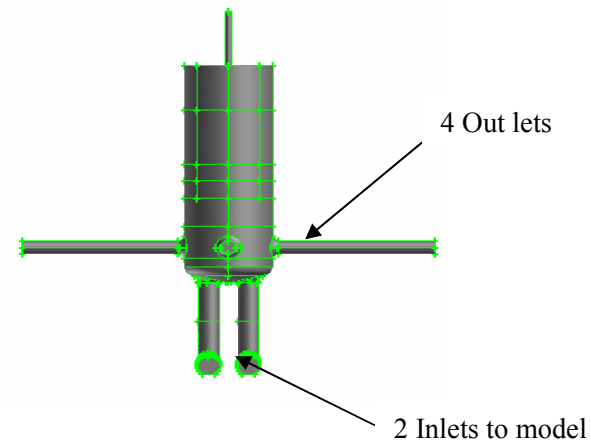

Fig.2 Geometry of CFD model

4.1 Numerical Procedure

4.1.1 Mass conservation equation

The equation for conservation of mass, or continuity equation, can be written as follows

$$\frac{\partial \rho}{\partial t} + \nabla \cdot (\rho \vec{v}) = S_m \tag{3}$$

Equation is the general form of the mass conservation equation and is valid for incompressible as well as compressible flows. The source S_m is the source term.

4.1.2 Momentum conservation equations

A single momentum equation is solved throughout the domain, and the resulting velocity field is shared among the phases. The momentum equation, shown below, is dependent on the volume fractions of all phases through the properties ρ and μ.. Conservation of momentum is described by

$$\frac{\partial}{\partial t}(\rho \vec{v}) + \nabla \cdot (\rho \vec{v}\vec{v}) = -\nabla p + \nabla \cdot (\bar{\bar{\tau}}) + \rho \vec{g} + \vec{F} \tag{4}$$

where, **p** is the static pressure, $\bar{\bar{\tau}}$ is the stress tensor (described below), and $\rho \vec{g}$ and $\vec{F}$ are the gravitational body force and external body forces (e.g., that arise from interaction with the dispersed phase), respectively. $\vec{F}$ also contains other model-dependent source terms such as porous-media and user-defined sources. The stress tensor $\bar{\bar{\tau}}$ is given by

$$\bar{\bar{\tau}} = \mu \left[(\nabla \vec{v} + \nabla \vec{v}^{\,\mathrm{T}}) - \frac{2}{3} \nabla \cdot \vec{v} I \right] \tag{5}$$

Where μ is the molecular viscosity, I is the unit tensor, and the second term on the right hand side is the effect of volume dilation.

4.1.3 Transport equations for the RNG k- ϵ Model (Turbulence model)

The RNG k- ϵ model has a similar form to the standard k- ϵ model

$$\frac{\partial}{\partial t}(\rho k) + \frac{\partial}{\partial x_i}(\rho k u_i) = \frac{\partial}{\partial x_j}\left(\alpha_k \mu_{\text{eff}} \frac{\partial k}{\partial x_j}\right) + G_k + G_b - \rho\epsilon - Y_M + S_k \tag{6}$$

$$\frac{\partial}{\partial t}(\rho \epsilon) + \frac{\partial}{\partial x_i}(\rho \epsilon u_i) = \frac{\partial}{\partial x_j}\left(\alpha_\epsilon \mu_{\text{eff}} \frac{\partial \epsilon}{\partial x_j}\right) + C_{1\epsilon}\frac{\epsilon}{k}(G_k + C_{3\epsilon}G_b) - C_{2\epsilon}\rho\frac{\epsilon^2}{k} - R_\epsilon + S_\epsilon \tag{7}$$

In these equations, G_k represents the generation of turbulence kinetic energy due to the mean velocity gradients. G_b is the generation of turbulence kinetic energy due to buoyancy. Y_M represents the contribution of the fluctuating dilatation in compressible turbulence to the overall dissipation rate. The quantities α_k and α_ε are the inverse effective Prandtl numbers for k and ϵ, respectively. S_k and S_ε are user-defined source terms.

4.1.4 Volume fraction Equation

The tracking of the interface(s) between the phases is accomplished by the solution of a continuity equation for the volume fraction of one (or more) of the phases. For the **q** th phase, this equation has the following form

$$\frac{\partial \alpha_q}{\partial t} + \vec{v} \cdot \nabla \alpha_q = \frac{S_{\alpha_q}}{\rho_q} \tag{8}$$

By default, the source term on the right-hand side of equation is zero, but one can specify a constant or user-defined mass source for each phase as and when needed. The volume fraction equation will not be solved for the primary phase; the primary-phase volume fraction will be computed based on the following constraint

$$\sum_{q=1}^{n} \alpha_q = 1 \tag{9}$$

4.1.5 Properties

The properties appearing in the transport equations are determined by the presence of the component phases in each control volume. In a two-phase system, for example, if the phases are represented by the subscripts 1 and 2, and if the volume fraction of the second of these is being tracked, the density in each cell is given by

$$\rho = \alpha_2 \rho_2 + (1 - \alpha_2)\rho_1 \tag{10}$$

In general, for an n-phase system, the volume-fraction-averaged density, ρ takes on the following form. All other properties (e.g., viscosity) are computed in this manner

$$\rho = \sum \alpha_q \rho_q \tag{11}$$

4.2 Analysis and Results

Geometrical modeling was carried out using GAMBIT, the pre processor of FLUENT, a Finite Volume Based CFD Package. A complete time-dependent solution of the exact Navier-Stokes equations for high-Reynolds-number turbulent flows in complex geometries is unlikely to be attainable for some time to come. Reynolds averaging is one of the alternative methods that can be employed to transform the Navier-Stokes equations in such a way that the small-scale turbulent fluctuations do not have to be directly simulated. The Reynolds-averaged Navier-Stokes (RANS) equations represent transport equations for the mean flow quantities only, with all the scales of the turbulence being modeled. The approach of permitting a solution for the mean flow variables greatly reduces the computational effort. The mean flow is assumed steady and a steady-state solution can be obtained economically. The Reynolds-averaged approach is generally adopted for practical engineering calculations and hence for the present case also. All the cases were simulated using multi phase Volume of Fluid (VOF) modeling. VOF simulation is capable of tracking the interfaces without excessive numerical diffusion. The cases considered for the study are of two-phase flow with air cushion above water for various flow rates, different free level heights and different air pressures. At the inlet, flow rate is specified and the flows through the four outlets are equal.

Some of the cases (1-15) analyzed are shown in Table -1. For cases 1-14, free surface is open to atmosphere and for the case 15 the air pressure of 0.2 bar is applied above the free surface of water. For turbulence modeling, RNG k-ε modeling is used. These cases are analyzed to find out whether there is any air entrainment into water under steady state conditions of operation by observing unsteadiness in the solution behaviour.

Table-1 Summary of Computation performed

Sl. No.	Geometry & cases analyzed	Flow rate m^3/h	Height of water (m)	Details of devices & Cover gas pressure (Atmosphere pressure for cases 1 to 14)
1	Case-1	2000	1.5	With out any internal devices
2	Case-2	2200	1.5	10% Porous plate (P.P)
3	Case-3	2200	1.5	20% Porous plate
4	Case-4	2200	1.5	30% Porous plate
5	Case-5	3570	1.5	30% P.P + 30 deg ring @ 1.5 D
6	Case-6	3670	2.0	30% P.P + 90 deg ring@ 1.5 D
7	Case-7	3560	1.5	30% P.P + 45 deg ring@ 1.5 D
8	Case-8	3690	1.8	20% P.P + 30 deg ring@ 1.5 D
9	Case-9	3560	1.5	20% P.P + 45 deg ring@ 1.5 D
10	Case-10	3595	1.5	20% P.P+ 90 deg Stiffener plate Ring ID=826 @ 1.5 D
11	Case-11	3590	1.5	20% P.P+ 30 deg ring @ 1.5 D + additional ring Ring ID=826 @ 3D
12	Case-12	3590	1.5	20% Porous plate + two rings (Ring ID=826 & 816.4 mm) @ 1.5D ,@ 3D
13	Case-13	3650	1.5	Pepper pot alone (450 mm)
14	Case-14	3650	1.5	Pepper pot (450mm) + 20% P.P
15	Case-15	3700	1.2	Pepper pot (450mm) + Ring type perforated cylindrical shell Ring ID=826 @ 1.5 D (0.2 bar cover gas pressure)

Maximum free surface velocity was determined for various cases using single phase simulation. It was found from the analysis that in Case1 (without any internal device), water and air is mixing well in the tank. For Cases 2-4 (with porous plates, refer Table-1), the flow pattern had slightly improved when compared to case-1. Typical simulation plots for 20% porous plate (case 3) is shown in Fig.3a and 3b.

The geometry was further modified as shown in case 11 and 12. Apart from the porous plate, two additional devices, namely 30 deg stiffener ring and ring plate, were introduced above the outlets in Case-11. Whereas in case-12, two ring plates of different inner diameter was introduced at 1.5Dout and 3.0Dout locations from the centre of the outlet. Fig 4a & 4b shows a typical plot for case-12. The analysis indicated a further reduction in the free surface velocity when compared to the earlier cases. However it was still not possible to completely eliminate entrainment.

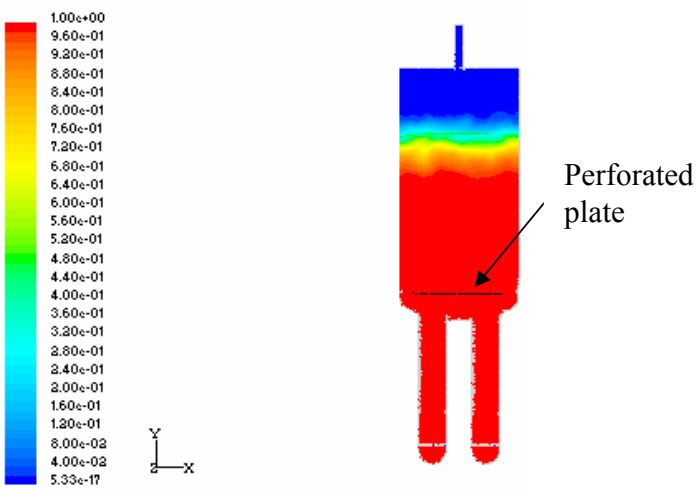

Fig.3a Contours of volume fractions of water in normal plane between two outlets (Case-3)

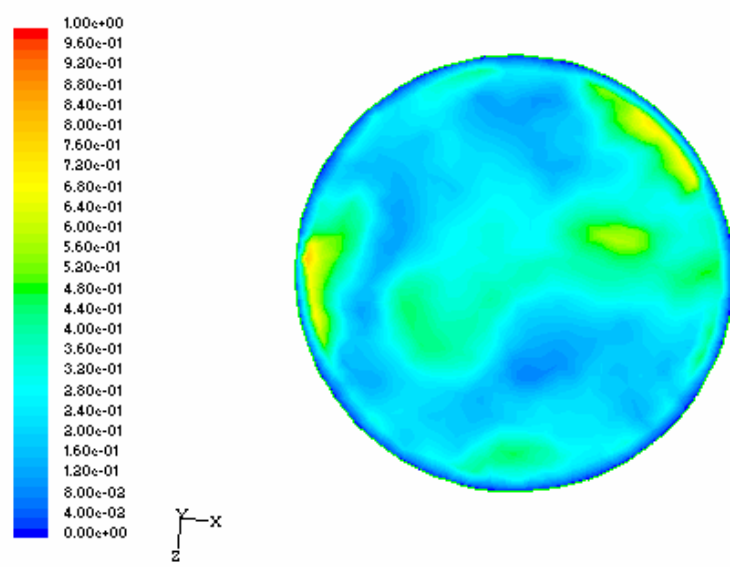

Fig.3b Contours of velocity at the interface in m/s (case-3)

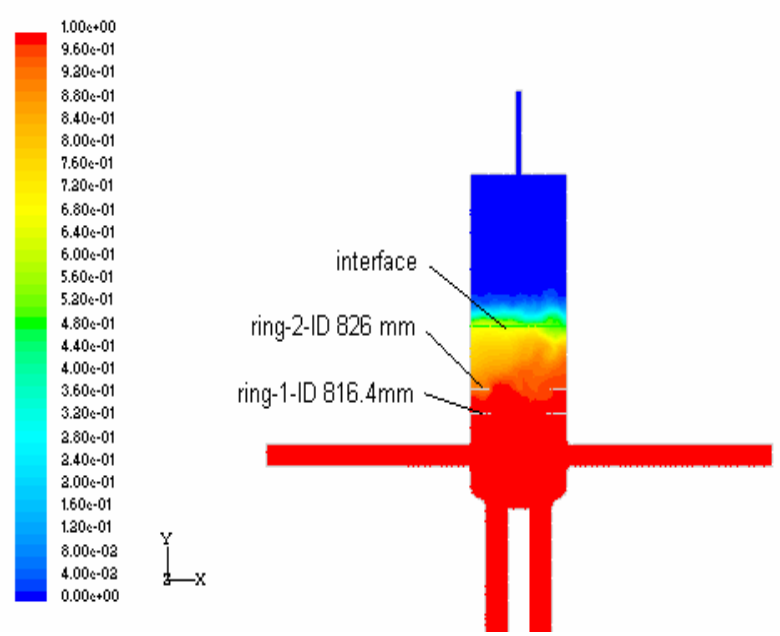

Fig.4a Contours of volume fraction of water (Case-12)

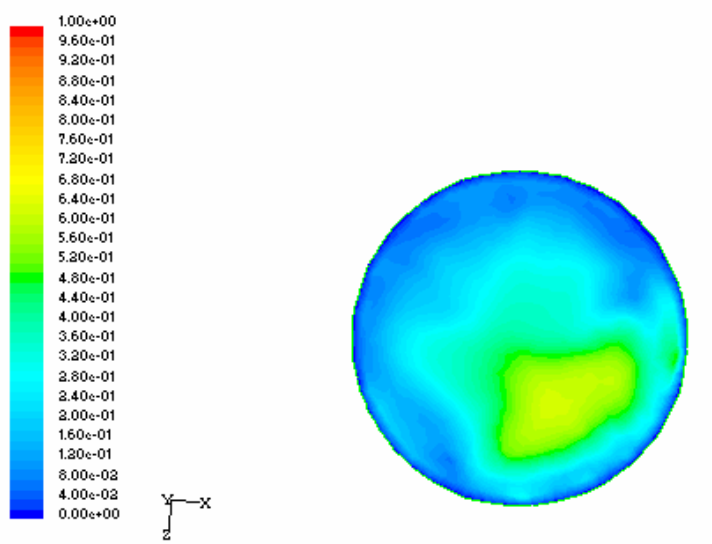

Fig. 4b Velocity contours at the interface (Case-12)

For minimizing the free surface velocity and height of the liquid column, a new device namely pepper pot, was introduced above the inlet nozzles (Case-13). The analysis with this device also indicated that air entrainment was still prevalent at the maximum flow rate. In case-14 a porous plate (porosity 20%) was provided in the surge tank above the outlet nozzles in addition to the pepper pot. It was observed that flow pattern improved in the above case but flow lines indicated air entrainment. Hence geometry was further modified (Case-15) by providing a ring type cylindrical perforated shell in the surge tank above the outlets in addition to the pepper pot as in case-13. From Fig 5a & 5b, it is inferred that the free surface velocity has reduced to a minimum of 0.28 m/s. The maximum void fraction at minimum water level is 3.5% and also very much

reduced. Finally case-15 geometry has been selected as the optimized geometry for mitigating air entrainment

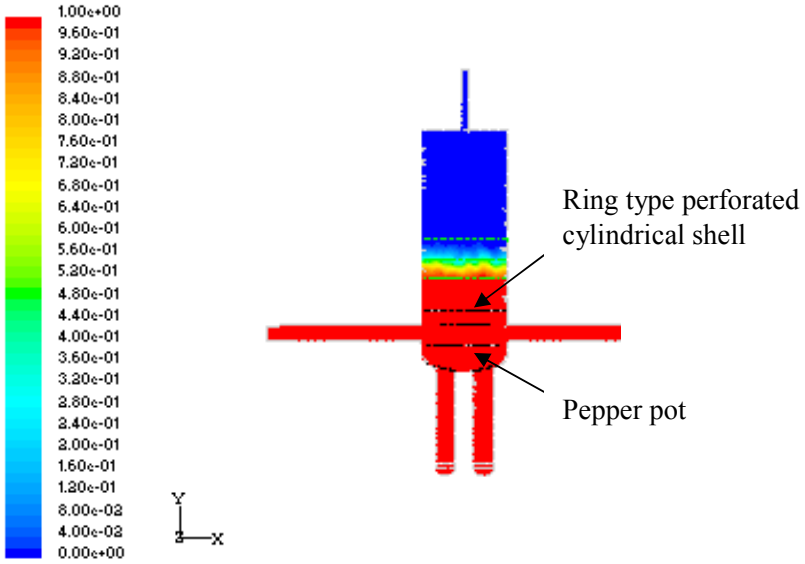

Fig-5a Contours of volume fraction of water (Case-15)

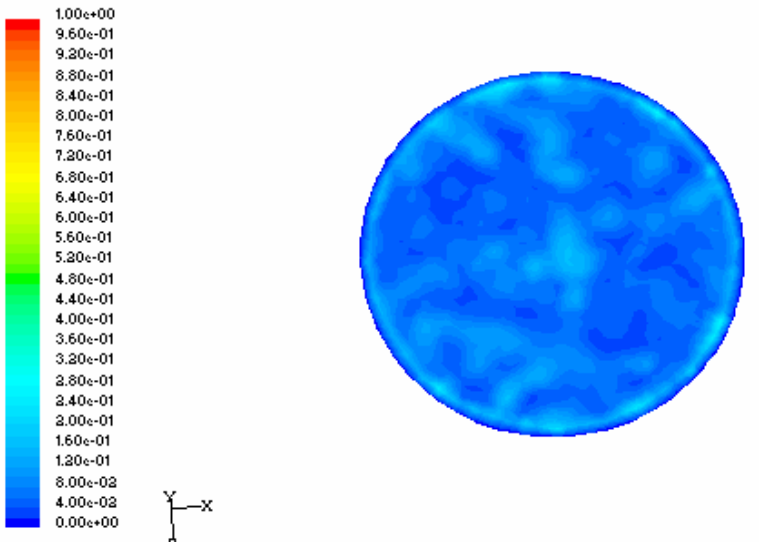

Fig- 5b Velocity contours at the interface (Case-15)

5.0 EXPERIMENTAL MODEL DETAILS

Studies were conducted in a 5/8 scale model of the prototype and geometric similarity was maintained between the model and prototype. Surge tank model comprises of a torispherical dished at the bottom with two inlet nozzles and a cylindrical shell above the dished end with four outlet nozzles. Stainless steel was used for the fabrication of the surge tank. Perspex windows were provided to visualize the free surface behaviour and air bubble entrainment in model. Fig. 6 shows the details of the model and setup.

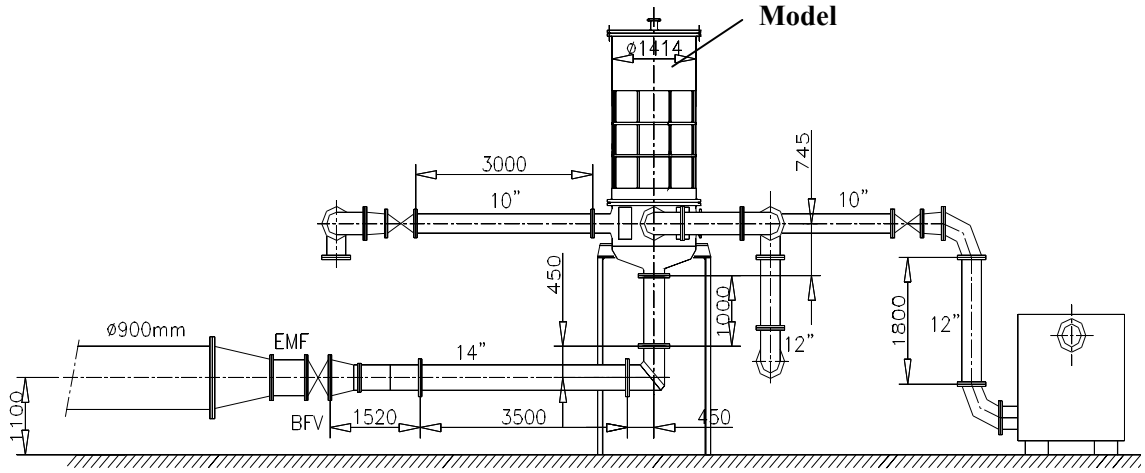

Fig.6. Schematic of 5/8 scale surge tank model set up

6.0 TEST LOOP DETAILS & EXPERIMENTAL METHODOLOGY

A test loop as shown in Fig. 6 was set up for this study. To carry out the study centrifugal pumps were utilized with different ranges to deliver flow to the model from a storage tank. Two calibrated average pitot tube flow meters were installed in parallel to measure the flow entering into the model through the two inlet nozzles. Each of the 4 outlet nozzles has a controlling valve to throttle the outlet flow from the model. Flow from each of the four outlets is discharged back into the storage tank.

The study involves establishing the minimum free surface of the liquid in the surge tank without any gas entrainment for nominal flow condition. Initially, nominal flow is set in the surge tank and the height of the liquid column is recorded. Surface activities such as formation of vortices at the free surface, free level fluctuations and gas entrainment phenomenon were observed and recorded. Similar methodology was adopted for different flow rates and for different air pressures applied over the liquid surface

6.1 Instrumentation

The gas entrainment phenomenon was observed visually with naked eye and the same also was recorded with a high speed camera and camcorder. The flow rate through the inlet (nominal flow rate 2500m3/h) and outlet nominal flow rate 1250m3/h) nozzles was measured using site calibrated averaging Pitot tubes and differential pressure transmitters. Pressure transmitters with measuring range of 0-5 m WC, resolution 0.1% and uncertainty 0.5% of reading was employed. A multiplexing system was employed for differential pressure sensing of the two inlet & four outlet nozzles. Total flow into the surge tank was measured with an Electromagnetic flow meter (range of 5000 m3/h, resolution 0.1% and uncertainty 0.25% of reading).

Static pressure was monitored using calibrated pressure transducers (range 0-4 bar for inlet & 0-2 bar for outlet, resolution 0.5 % of reading) with suitable multiplexing mechanism. Pressure

gauges were also provided. The water temperature was monitored using an RTD and Indicator. Level of water in the tank was monitored using a ultrasonic based level indicator (range of 0 – 4 m, resolution 0.01 m & uncertainty 0.5% of reading).

To sense pressure fluctuation caused by the entrained gas, dynamic pressure transducers were employed. Kistler piezo-electric transducers with a range of 0 – 2 bar and uncertainty 1% was employed and fitted flush with the inner wall of pipe. Photographs were taken to record the presence of air bubbles in the water during experiments.

Table-2 below shows the typical parameters measured during experimentation for the various cases studied. Tests were conducted with surge tank top surface open to atmosphere and also with cover gas pressure acting on the water surface. The cover gas pressure was simulated with compressed air above the free surface of water. The outlet flow in each channel, total flow, fluctuation in water level head of water column at the bottom of the surge tank were monitored after reaching steady state conditions. The details of measurements taken during trials were tabulated in table below. The presence of air bubbles were observed using videography. This was repeated for different configurations of the porous plate, stiffener ring and pepper pot.

Table –2 Test results with Porous Plates

Flow rate (m^3/hr)					Head	Cover gas Air Pressure	Fluctuation in level	Outlet velocity	Fr. No.
Ch #1	Ch #2	Ch #3	Ch #4	Total	m	bar	mm	m/s	
Porous plate with porosity =0.1									
Condition - Open to Atmosphere									
421	426	420	415	1700	1.4	0	35	2.454	1.324
520	510	500	520	2100	1.9	0	30	3.032	1.636
788	790	800	791	3150	2.2	0	30	4.547	2.454
Condition - with cover gas air pressure									
940	945	948	910	3741	2.7	0.2	25	5.400	2.914
740	730	735	720	2965	1.9	0.7	30	4.280	2.310
700	695	685	680	2816	1.88	0.7	25	4.065	2.194
Porous plate with porosity = 0.3									
526	530	532	552	2200	1.6	0	30	3.176	1.714
820	819	800	822	3250	1.9	0.1	25	4.692	2.532
955	949	942	960	3950	1.86	0.1	25	5.702	3.077
Condition - with cover gas air pressure									
770	762	780	773	3000	1.75	0.7	25	4.331	2.337
743	669	755	735	2900	1.676	0.6	20	4.186	2.259
625	632	626	620	2500	1.3	0.7	15	3.609	1.948

7.0 EXPERIMENTAL RESULTS

Preliminary studies were conducted without any device and later with different configuration of devices to determine the H/D. (the free level height of liquid column non-dimensionalised with respect to the surge tank diameter). The objective was to determine the maximum value of H/D at which gas entrainment is initiated for the operating Froude number of 3.1. To validate the CFD results, experiments were carried out with similar devices were used in the computational modeling. The devices are shown in Fig.7

Fig. 7 Devices used for experimental studies

Studies without any device indicated a H/D of 1.65 at 40% of the nominal flow. The impact of the incoming axial velocity component of the flow on the free surface causes turbulence and level fluctuations leading to gas entrainment. To reduce this liquid level, perforated plates were introduced above the inlet nozzle. This effected in reducing the level of liquid column considerably without any gas entrainment (Fig. 8). Though the direct impact on the liquid surface by the incoming fluid jet was reduced considerably due to presence of perforated plate, the axial velocity of the flow in the annulus area between the plate and tank was dominant causing surface level fluctuations and thus gas entrainment. The experimental uncertainty is ±2%

Reduction in this axial velocity component was achieved by positioning a stiffener ring inside the surge tank at 1.5D distance above the outlet nozzle. A combination of 20% perforated plate and a 30^{o} stiffener ring has helped in avoiding gas entrainment for H/D=1.53 at normal operating condition (Fig. 9). Studies with pepper pot device and ring type cylindrical perforated shell (Fig.10) has helped in avoiding gas entrainment for H/D=1.28 at nominal flow. (Ramdasu, 2007).

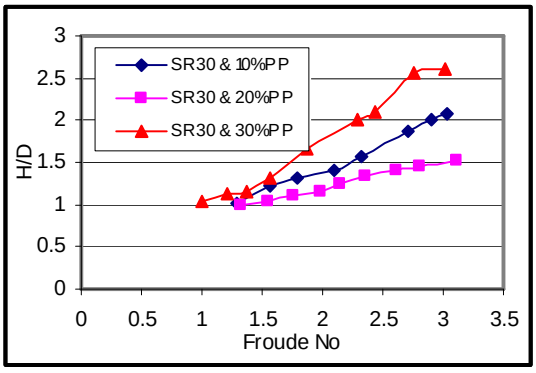

Fig. 8 Effect of perforated plate on H/D

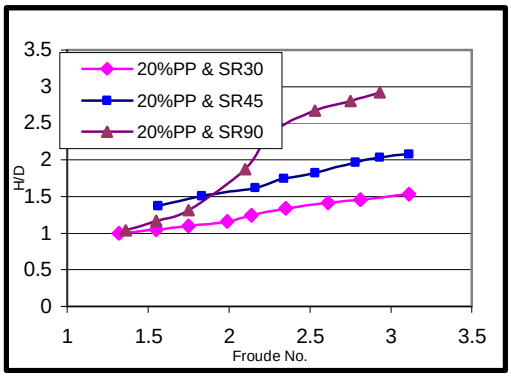

Fig. 9 Effect of stiffener rings on H/D

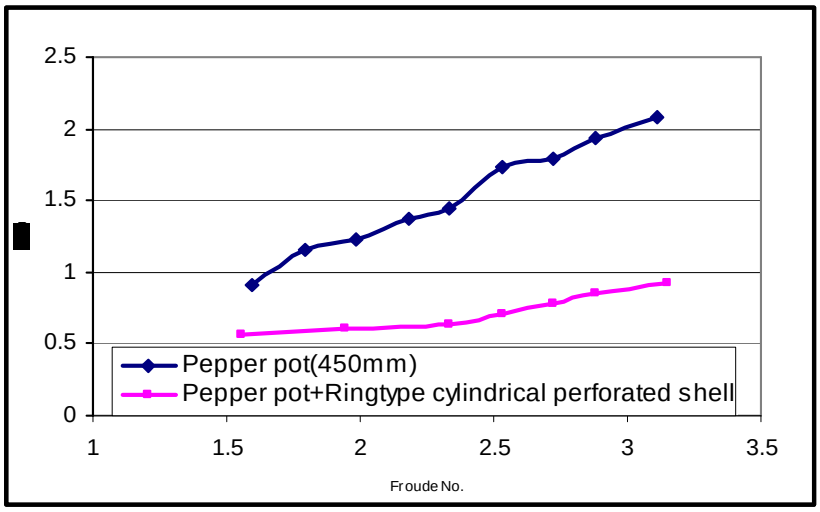

Fig.10 Effect of pepper pot and with ring type cylindrical perforated shell

8.0 COMPARISON OF RESULTS COMPUTATIONAL & EXPERIMENTAL

The results of the cases investigated experimentally were compared with the corresponding CFD results are shown in Fig.11. It is observed that the CFD and experimental results were in good agreement for most of the cases. For cases 2 and 13 the variation in H/D between CFD and experiments was higher (~ 28%) than the other cases. The results for case 15, the optimum geometry for mitigating gas entrainment was found to have close match between the CFD and experimental results.

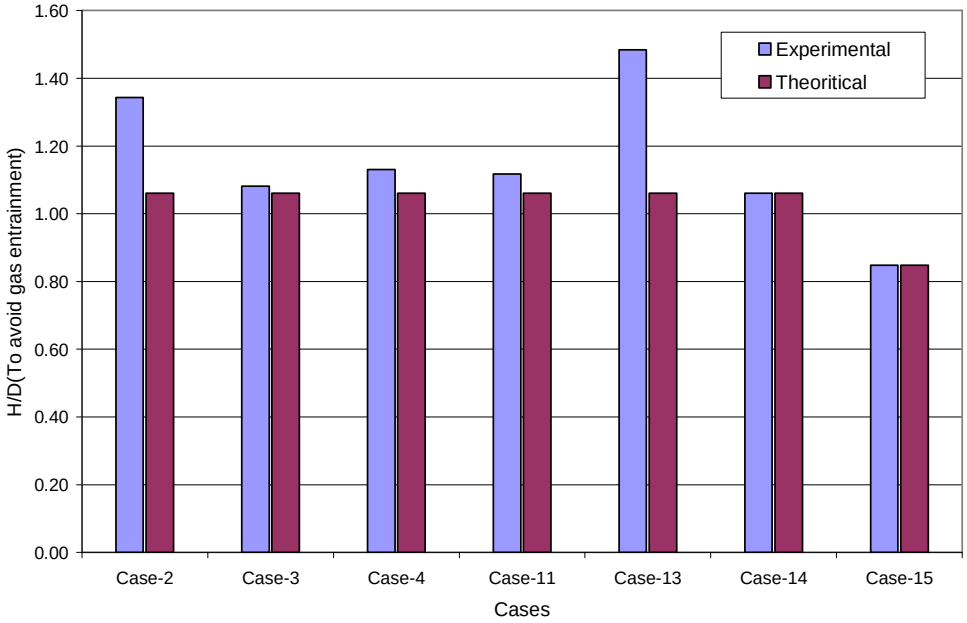

Fig.11 shows the H/D of CFD and experiments for typical cases

9.0 CONCLUSION

Computational modeling and experiments were carried out to study the phenomenon of gas entrainment in a 5/8 scaled 360 deg full circular model of PFBR surge tank. Minimum free level height required for avoiding gas entrainment and free surface velocities were determined for various combinations. The CFD analysis was beneficial in reducing the experimental trials using various device configurations. From the CFD analysis, the combination of Pepper pot with ring type cylindrical perforated shell was found to be the most effective in avoiding gas entrainment at H/D= 1.2. For the same configuration of the devices, the experiment also reported a H/D value of 1.28 which is in very close agreement with the CFD results. Further work is necessary to improve CFD prediction.

10.0 REFERENCES

1. Gao Ming Qing " Evaluation for the effects of a ring plate device to eliminate free surface gradients in Liquid Metal Fast Breeder Reactor vessel using multi-dimensional Thermal hydraulics computer code" PNC TN9410 97-016, February, 1997.

2. Ramdasu.D, N.S.Shivakumar, G. Padmakumar, C.Anand Babu & G.Vaidyanathan " Studies on Scaled Models for Gas Entrainment in the Surge Tank of LMFBR" Proceedings of ICAPP 2007 Nice, France, May 13-18, 2007 Paper 7048.

3. Tomaki Kinugi " Numerical study on onset of gas entrainment from free surface" 11th International Topical meeting on Nuclear Reactor Thermal Hydraulics (NURETH-11) Avignon, France, October 2-6 2005